

Motion Forcing: A Decoupled Framework for Robust Video Generation in Motion Dynamics

Tianshuo Xu¹, Zhifei Chen¹, Leyi Wu¹, Hao Lu¹, and Ying-cong Chen^{1,2,*}
<https://github.com/Tianshuo-Xu/Motion-Forcing>

¹ The Hong Kong University of Science and Technology (Guangzhou)

² The Hong Kong University of Science and Technology
 {txu647, zchen379}@connect.hkust-gz.edu.cn



Fig. 1: Our framework, **Motion Forcing**, taking user input motion and the first frame, generates motion-coherent future frames. (a-d) showcase the model’s ability to generate reactive ego-trajectories that respond dynamically to diverse dangerous scenarios initiated by other vehicles. (e) showcases a physics scene where different actions lead to different collision results. (f) illustrates embodied AI, where providing different directional inputs allows a robotic hand to move an object in the corresponding directions. **Full videos are available at the project repository.**

Abstract. The ultimate goal of video generation is to satisfy a fundamental trilemma: achieving high visual quality, maintaining rigorous physical consistency, and enabling precise controllability. While recent models can maintain this balance in simple, isolated scenarios, we observe that this equilibrium is fragile and often breaks down as scene complexity increases (e.g., involving collisions or dense traffic). To address this, we introduce **Motion Forcing**, a framework designed to stabilize this trilemma even in complex generative tasks. Our key insight is to explicitly decouple

*Corresponding author.

physical reasoning from visual synthesis via a hierarchical “**Point-Shape-Appearance**” paradigm. This approach decomposes generation into verifiable stages: modeling complex dynamics as sparse geometric anchors (**Point**), expanding them into dynamic depth maps that explicitly resolve 3D geometry (**Shape**), and finally rendering high-fidelity textures (**Appearance**). Furthermore, to foster robust physical understanding, we employ a **Masked Point Recovery** strategy. By randomly masking input anchors during training and enforcing the reconstruction of complete dynamic depth, the model is compelled to move beyond passive pattern matching and learn latent physical laws (e.g., inertia) to infer missing trajectories. Extensive experiments on autonomous driving benchmarks show that Motion Forcing significantly outperforms state-of-the-art baselines, maintaining trilemma stability across complex scenes. Evaluations on physics and robotics further confirm our framework’s generality.

Keywords: Video Generation · Autonomous Driving · Physical Consistency · Controllable Generation

1 Introduction

Recent advances in video generation [3,9,14,49,50] have achieved remarkable levels of perceptual fidelity, revolutionizing fields from entertainment [16,51,58] to virtual reality [4,23,55]. However, a significant gap remains between visual realism and physical consistency. While current models excel at synthesizing high-resolution textures and lighting, they frequently violate fundamental physical laws—such as inertia, collision dynamics, and object permanence—when generating complex motions [1,17,28]. This limitation presents a critical bottleneck for "world models" in safety-centric domains like autonomous driving [15,21,42,47,57] and robotics [12,18,45], where predictive models must not only look plausible but also adhere to rigorous physical constraints to support reliable decision-making.

We attribute this inconsistency to the *entanglement* within end-to-end models. By unifying dynamics and appearance, models inherently prioritize high-frequency visual details—easier to minimize in loss functions—over long-term physical consistency. While frameworks like MoFA-Video [31] and STANCE [10] attempt to mitigate this by introducing motion intermediates, they fundamentally struggle to bridge the substantial domain gap between sparse signals and dense video. Specifically, MoFA-Video relies on coarse optical flow combined with Softmax Splatting; this mismatch between rough control signals and a pixel-precise warping mechanism leads to degraded controllability in complex scenes, where the model ignores user guidance to preserve visual stability. Similarly, STANCE attempts to generate RGB video directly—relying on auxiliary motion losses as soft constraints—which leaves the vast learning gap between sparse control and dense pixels unbridged. Consequently, in scenarios with high complexity, both methods are forced into a trade-off, unable to simultaneously maintain rigorous physical consistency and precise response to user commands.

To overcome these limitations without relying on intricate control strategies like Softmax Splatting [31,50], we propose **Motion Forcing**, a streamlined frame-

work built upon a novel “**Point-Shape-Appearance**” hierarchical paradigm. Inspired by the principles of Diffusion Forcing [7], we decompose the complex video generation problem into three progressively dense stages with minimal domain gaps: (i) **Point**: we abstract each object as a positional anchor carrying global scale attributes (derived from the inscribed circle) to encode depth ordering; (ii) **Shape**: we generate dynamic *depth maps* that capture continuous 3D surface geometry, providing a substantially richer structural prior for resolving physical interactions such as occlusion, collision, and relative motion in 3D space; and (iii) **Appearance**: we render high-fidelity RGB frames conditioned on the verified geometric layout. By forcing the model to infer the intermediate geometric “Shape” from sparse “Points” before hallucinating pixels, we ensure that the physical skeleton of the scene is established at a 3D-aware structural level, bridging the domain gap between sparse control cues and dense video with a physically grounded intermediate representation.

To foster active physical reasoning over passive control, we employ a **Masked Point Recovery** strategy. During training, we randomly mask input **points** and require the model to reconstruct the underlying dynamic depth sequence (Shape). This objective compels the network to internalize physical dynamics—such as inertia, depth ordering, and object permanence—to infer plausible missing trajectories in 3D space. By recovering continuous global geometry from partial spatial cues, our model guarantees that the generated content adheres to physical constraints while remaining precisely controllable, simultaneously achieving high visual fidelity and logical coherence. Moreover, adopting points as the foundational control primitive offers exceptional flexibility. Trajectories can be readily instantiated from diverse inputs—ranging from user-drawn arrows to language instructions—via standard temporal interpolation scripts. Crucially, this formulation supports the explicit modulation of derivatives, allowing users to fine-tune kinematic properties (e.g., instantaneous velocity) at each timestep for granular dynamic manipulation.

We empirically validate Motion Forcing primarily on complex autonomous driving scenarios (using a curated dataset sourced from Waymo [36], Driving Dojo [44], and YouTube), and further demonstrate the generality of our framework on object dynamics (Physion [2]) and robotic manipulation (Jaco Play [11]). Through extensive qualitative and quantitative comparisons against state-of-the-art editing models (e.g., MoFA-Video [31]), domain-specific generators, and leading foundation models—including the powerful closed-source Seed-Dance 2.0 [37] and the advanced Wan 2.6 [38]—we demonstrate that our approach significantly improves physical plausibility and motion coherence without compromising visual fidelity. Notably, our method proves robust in complex multi-object settings where baseline control mechanisms typically degrade, effectively resolving the trade-off between controllability and physical consistency.

In summary, our contributions are threefold:

- **Motion Forcing Framework.** We propose a novel decoupled generation paradigm that resolves the entanglement of dynamics and appearance found in end-to-end models. By structuring generation into a “**Point-Shape-**

- Appearance**” hierarchy, we bridge the domain gap between sparse cues and dense video, enforcing logical consistency before rendering pixels.
- **Active Reasoning via Masked Point Recovery.** We introduce a Masked Point Recovery strategy that elevates the model from passive instruction-following to active physical reasoning. By forcing the reconstruction of dynamic shapes from sparse, randomly masked geometric anchors, our model internalizes fundamental physical laws (e.g., inertia) to infer plausible trajectories.
 - **Unified Flexibility and Precision.** We demonstrate that our point-based control primitive supports diverse inputs—from user sketches to script-based kinematic modulation—offering a unified solution that achieves state-of-the-art performance on autonomous driving benchmarks, with strong generalization to physics simulation and robotic manipulation.

2 Related Work

2.1 Video Diffusion Models

Video generation models predominantly extended UNet-based latent diffusion models (LDMs) from text-to-image frameworks like Stable Diffusion [35] to accommodate video applications. For instance, AnimateDiff [13] introduced a temporal attention module to enhance temporal consistency across frames. Building upon this, subsequent video generation models [5, 8, 9, 41, 52, 53] adopted alternating attention mechanisms that combine 2D spatial attention with 1D temporal attention. Notable examples include ModelScope, VideoCrafter, Moonshot, and Show-1, which have demonstrated significant improvements in video generation.

More recently, the field has undergone a significant paradigm shift from UNet backbones toward Diffusion Transformers (DiT) to better scale model capacity and capture complex spatiotemporal dependencies. Foundational models such as Sora [32], CogVideoX [49], HunyuanVideo [19], and Wan 2.1 [38] leverage large-scale DiT architectures often combined with Flow Matching [22] frameworks. By employing 3D causal convolutions and sophisticated rotary positional embeddings, these models significantly improve motion coherence and text-to-video alignment, pushing the boundaries of high-resolution, long-duration video synthesis.

2.2 Controllable Motion Generation

Controllable motion generation in video synthesis aims to produce videos that not only exhibit high visual quality but also adhere to specified motion patterns and dynamics. Prior works [46, 50] allow users to specify motion trajectories directly, enabling fine-grained control over the path an object takes in the video. Others utilize keypoints or motion fields to guide animations, translating abstract motion representations into realistic movements [30, 31]. By integrating these control mechanisms, these approaches aim to bridge the gap between user intent and the generated content.

Recently, a novel category of video generation models, referred to as “world models,” has emerged [15,21,42,43,47,57]. Pioneering models like DriveDreamer [42] and DriveDiffusion [21] employ diffusion models conditioned on layout and ego-action to generate controllable driving videos. GAIA-I [15] further expands this paradigm by incorporating multiple conditioning inputs, such as video, text, layouts, and actions, enabling the generation of realistic and diverse driving scenarios with fine-grained control over vehicle behavior and scene features. GenAD [47] advances these efforts by scaling both the video prediction model and the dataset, thereby effectively managing complex driving scene dynamics. More recently, Gen3C [34] and NeoVerse [48] introduce 3D-informed caches and monocular 4D world models to enhance temporal and geometric consistency. Similarly, PhiGenesis [27] and GeoDrive [6] explicitly integrate stereo forcing or geometric constraints to ensure precise action control and 3D structural fidelity in driving scenes.

2.3 Physically Coherent Video Generation

While mainstream video models achieve high perceptual fidelity, they frequently violate fundamental physical laws [1, 29]. Recent research addresses this gap through three primary streams. First, hybrid approaches like PhysGen [25] integrate explicit physics engines. However, reliance on external simulators limits their generalization to complex, in-the-wild scenarios lacking pre-defined parameters. Second, physics-aware reasoning methods [54,56] leverage LLMs or VFMs to infer physical events (e.g., collisions) and guide diffusion via textual or attention-based cues. Third, latent-based approaches [10,20] embed physics priors directly into latent spaces or explicitly model attributes like mass to constrain object motion and dynamics.

Despite these advancements, the inherent entanglement of dynamics and appearance remains a critical bottleneck. Treating physical constraints as auxiliary losses in end-to-end frameworks often allows visual details to override long-term consistency, causing failures in object permanence and collision dynamics. In contrast, our approach resolves this trade-off by explicitly decoupling physical reasoning from visual rendering, verifying the scene’s geometric “skeleton” before pixel synthesis.

3 Method

Generating controllable autonomous driving videos requires jointly reasoning about two intertwined but distinct aspects of scene evolution: *where things move* (physical dynamics) and *what things look like* (visual rendering). Attempting to map sparse control signals \mathbf{P} directly to dense video pixels \mathbf{V} conflates these challenges, forcing a model to simultaneously resolve global 3D geometry and hallucinate local texture within a single generation step. We address this by introducing **Depth** as an intermediate structural representation, decomposing generation into *Physical Reasoning* ($\mathbf{P}, \mathbf{C} \rightarrow \mathbf{D}$) and *Neural Rendering* ($\mathbf{D} \rightarrow$

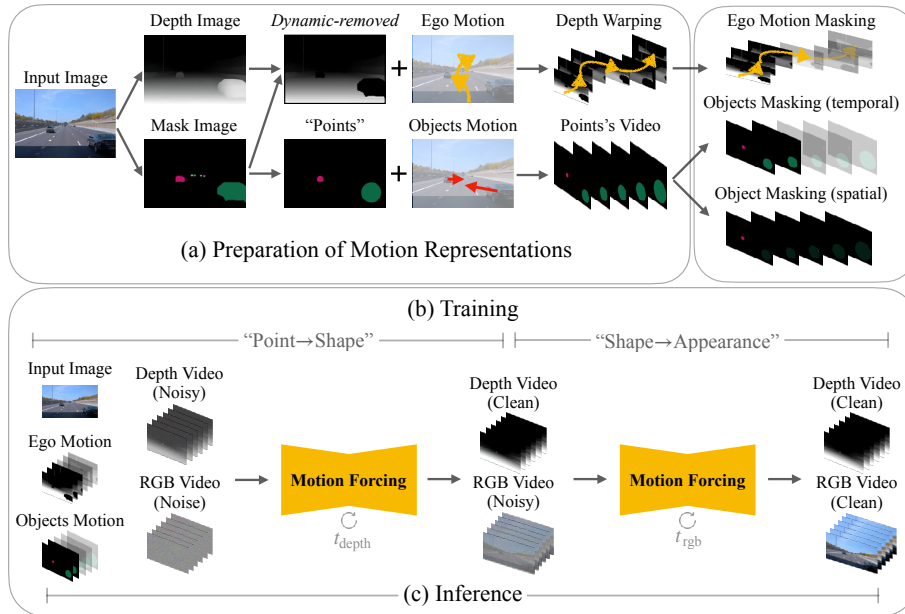


Fig. 2: Overview of the Motion Forcing framework. (a) Preparation of Motion Representations: Input control signals are processed and subjected to spatial and temporal masking before being fed into the model. **(b) Training:** The model is trained by randomly sampling between two independent stages: "Point \rightarrow Shape" (depth generation) and "Shape \rightarrow Appearance" (RGB rendering). **(c) Inference:** The generation follows a complete two-stage hierarchical process, sequentially mapping sparse points to structural depth (Shape), and finally to the target RGB video (Appearance).

\mathbf{V}), where \mathbf{C} denotes camera motion. Crucially, both stages share a single unified diffusion backbone, enabling knowledge transfer between dynamics and appearance while eliminating cascading error propagation.

In this section, we formalize the representations and problem setup (Sec. 3.1), describe camera motion encoding via depth warping (Sec. 3.2), the hierarchical diffusion forcing formulation (Sec. 3.3), the masked point recovery strategy (Sec. 3.4), and the inference pipeline (Sec. 3.5).

3.1 Preliminaries

Given a reference image \mathbf{I}_0 and a sequence of sparse control signals, our goal is to generate a physically plausible driving video $\mathbf{V} = \{\mathbf{I}_t\}_{t=0}^T$ that faithfully follows the prescribed vehicle motions and camera trajectory. We formulate this as a hierarchical mapping across three levels of scene description:

- **Point** $\mathbf{P} = \{\mathbf{P}_t\}_{t=0}^T$: The sparse control signal for dynamic agents. Each tracked object i at frame t is abstracted as its *maximum inscribed circle*,

parameterized by a centroid (x_t^i, y_t^i) and radius r_t^i . These are rendered as colored primitives on a canvas and encoded via the VAE. The centroid governs planar motion while the radius implicitly encodes depth via perspective projection, offering both geometric explicitness and procedural flexibility for scripting kinematic profiles.

- **Depth \mathbf{D}** = $\{\mathbf{D}_t\}_{t=0}^T$: The intermediate structural representation consisting of temporally-consistent dense depth maps. Unlike instance segmentation, depth captures continuous 3D scene geometry—encoding surface distances, spatial relationships, and occlusion ordering in a unified metric space. This makes it a natural bridge between control-level reasoning and pixel-level rendering.
- **Appearance \mathbf{V}** = $\{\mathbf{I}_t\}_{t=0}^T$: The target RGB video containing high-frequency visual details—texture, lighting, shadows, and material properties.

In addition to agent-level control, driving scenarios require explicit camera motion specification. We denote the camera trajectory as $\mathbf{C} = \{(\mathbf{R}_t, \mathbf{t}_t, \mathbf{K}_t)\}_{t=0}^T$, comprising per-frame extrinsics $[\mathbf{R}_t | \mathbf{t}_t] \in \mathbb{R}^{3 \times 4}$ and intrinsics $\mathbf{K}_t \in \mathbb{R}^{3 \times 3}$, estimated by VGGT [40]. We next describe how \mathbf{C} is encoded into a form compatible with our depth-centric framework.

3.2 Camera Motion via Depth Warping

A standard approach to injecting camera motion into a diffusion model is to embed the extrinsic parameters $(\mathbf{R}_t, \mathbf{t}_t)$ and intrinsics \mathbf{K}_t as global conditioning vectors via cross-attention or adaptive normalization. However, this parametric strategy faces two critical challenges in the driving domain.

First, **entanglement under limited data diversity**. When camera pose is injected as a low-dimensional embedding alongside other conditions (e.g., the reference image, text, or layout), the model tends to entangle camera motion with scene content rather than learning a clean, disentangled control axis. This problem is exacerbated in driving datasets, where camera trajectories are strongly correlated with scene layout and agent behavior, making factorization exceptionally difficult without massive data diversity.

Second, **insufficient spatial precision for 3D-grounded control**. Autonomous driving demands geometrically precise camera manipulation in 3D space. A parametric embedding compresses the full 6-DoF transformation into a compact vector that the network must internally re-expand into dense, per-pixel displacements—a lossy bottleneck that is poorly suited to the pixel-aligned processing of convolutional and attention-based architectures.

To simultaneously address these issues, we propose representing camera motion as **warped depth maps**. By geometrically warping the first-frame depth \mathbf{D}_0 according to the target camera pose, we produce a dense, pixel-aligned conditioning signal. This representation is (i) *structurally decoupled* from appearance and layout conditions by construction, as it encodes only geometric camera effects, and (ii) spatially precise, making the full 6-DoF transformation explicit at every pixel location. Furthermore, since our intermediate representation

is also depth-based, encoding camera motion in the same modality establishes a shared geometric vocabulary. This is significantly easier for the network to internalize than bridging the gap between abstract pose parameters and pixel-space effects.

Formally, given the first-frame depth \mathbf{D}_0 and camera poses $\{(\mathbf{R}_t, \mathbf{t}_t, \mathbf{K}_t)\}_{t=0}^T$, we construct the camera motion conditioning $\mathbf{W} = \{\mathbf{W}_t\}_{t=0}^T$ by unprojecting the first-frame depth into 3D, transforming it to each target camera, and forward-splatting:

$$\mathbf{W}_t = \text{Splat}(\mathbf{D}_0, \Pi_t \circ \Pi_0^{-1}(\mathbf{u}, \mathbf{D}_0(\mathbf{u}))). \quad (1)$$

Concretely, for each pixel $\mathbf{u} = (u, v)$ in frame 0, we first unproject to a world-space point:

$$\mathbf{p}_{\text{world}} = \mathbf{R}_0^\top \left(\mathbf{D}_0(\mathbf{u}) \cdot \mathbf{K}_0^{-1} \begin{bmatrix} u \\ v \\ 1 \end{bmatrix} - \mathbf{t}_0 \right), \quad (2)$$

and then project it onto frame t 's image plane:

$$\mathbf{u}_t = \pi(\mathbf{K}_t(\mathbf{R}_t \mathbf{p}_{\text{world}} + \mathbf{t}_t)), \quad (3)$$

where π denotes perspective division. Finally, the depth value $\mathbf{D}_0(\mathbf{u})$ is splatted to location \mathbf{u}_t in the target frame.

3.3 Motion Forcing: Unified Hierarchical Diffusion

Rather than cascading separate models for reasoning and rendering, we propose a **single unified diffusion model** ϵ_θ that handles both stages within a shared 3D DiT backbone [49]. The key mechanism enabling this is **dual independent diffusion timesteps**: τ_d controls the noise level of the depth latents, and τ_v controls the noise level of the video latents.

Let $\mathbf{z}_{\tau_d}^d$ and $\mathbf{z}_{\tau_v}^v$ denote the VAE-encoded latents of \mathbf{D} and \mathbf{V} , perturbed by Gaussian noise at levels τ_d and τ_v respectively. These latent streams are concatenated temporally and processed jointly by the backbone. Each stream is modulated by its specific timestep embedding via adaptive layer normalization (AdaLN), enabling disentangled denoising control. The unified objective is:

$$\mathcal{L} = \mathbb{E}_{\mathbf{D}, \mathbf{V}, \tau_d, \tau_v, \epsilon} \left[\left\| \epsilon - \epsilon_\theta(\mathbf{z}_{\tau_d}^d \oplus \mathbf{z}_{\tau_v}^v, \tau_d, \tau_v, \mathbf{I}_0, \mathbf{P}, \mathbf{W}) \right\|^2 \right], \quad (4)$$

where \oplus denotes temporal concatenation. The conditioning inputs—reference image \mathbf{I}_0 , point control \mathbf{P} , and camera depth \mathbf{W} —are each VAE-encoded and concatenated along the channel dimension of the noisy input.

Dual Adaptive Layer Normalization. To enable a single set of transformer blocks to simultaneously serve two denoising tasks, we extend the standard AdaLN mechanism. For each block, the depth and video halves of the hidden

state sequence receive *different* scale and shift parameters derived from their respective timestep embeddings τ_d and τ_v :

$$\mathbf{h}'_{1:T} = \text{LN}(\mathbf{h}_{1:T}) \odot [\gamma(\tau_d) \parallel \gamma(\tau_v)] + [\beta(\tau_d) \parallel \beta(\tau_v)], \quad (5)$$

where \parallel denotes concatenation along the temporal (sequence) axis, and γ, β are learned affine functions. At the output layer, `norm_out` is applied sequentially with both embeddings to produce the final prediction. This design allows the backbone attention layers to share representations while the normalization provides task-specific modulation.

Forcing Strategy. Inspired by Diffusion Forcing [7], we employ a **stochastic mode-switching** strategy. Each training iteration forces the model to solve exactly one sub-problem by fixing the non-target timestep:

- **Mode I: Physical Reasoning** (Point + Camera \rightarrow Depth). Set $\tau_v = T_{\max}$ (pure noise) and sample $\tau_d \sim \mathcal{U}\{0, \dots, T_{\max} - 1\}$. Deprived of RGB cues, the model reconstructs \mathbf{D} from the sparse control \mathbf{P} , camera depth \mathbf{W} , and reference \mathbf{I}_0 . This mode cultivates physical reasoning: inferring 3D structure evolution, resolving occlusions, and predicting dynamic depth changes from minimal control inputs.

$$\mathcal{L}_{\text{reason}} = \mathbb{E} \left[\|\epsilon_d - \hat{\epsilon}_d\|^2 \right], \quad \text{s.t. } \tau_v = T_{\max}. \quad (6)$$

- **Mode II: Neural Rendering** (Depth \rightarrow Appearance). Set $\tau_d = 0$ (ground truth) and sample $\tau_v \sim \mathcal{U}\{0, \dots, T_{\max} - 1\}$. Conditioned on perfect geometry, the model focuses on hallucinating consistent textures, lighting, and material properties:

$$\mathcal{L}_{\text{render}} = \mathbb{E} \left[\|\epsilon_v - \hat{\epsilon}_v\|^2 \right], \quad \text{s.t. } \tau_d = 0. \quad (7)$$

By alternating between modes, ϵ_θ learns to function as both a physics engine and a renderer within a shared latent space.

3.4 Masked Point Recovery for Physical Reasoning

To explicitly enforce causal reasoning and active physical understanding, we introduce **Masked Point Recovery**. A critical secondary objective of this strategy is to bridge the inherent gap between dense training trajectories and the sparse, partial inputs typical of real-world inference. By systematically corrupting input motion controls while strictly supervising on the complete intermediate depth video \mathbf{D} , we compel the model to internalize physical laws (e.g., inertia, object permanence) and hallucinate missing geometries. As shown in Fig. 2, we employ three distinct masking strategies:

Temporal Ego Masking We randomly truncate ego-motion conditioning. Camera signals after frame $t = \lfloor \tau_{\text{ego}} T \rfloor$, with a cutoff ratio $\tau_{\text{ego}} \sim \mathcal{U}(0.3, 1.0)$, are masked. The model must extrapolate the subsequent ego-trajectory from initial momentum and scene layout.

Temporal Object Masking Similarly, we apply a temporal mask to object control points \mathbf{P} beyond a sampled cutoff $\tau_{\text{obj}} \sim \mathcal{U}(0.3, 1.0)$, compelling the model to predict ongoing object motion from initial velocities.

Spatial Object Masking To model object permanence and implicit interactions, we independently drop the entire trajectory of each object i with probability p_{drop} :

$$m_{\text{spatial}}^{(i)} \sim \text{Bernoulli}(1 - p_{\text{drop}}). \quad (8)$$

The model must deduce the missing agent’s physical presence and trajectory from the target depth \mathbf{D} and the reactive behaviors of visible agents.

3.5 Inference: Two-Stage Hierarchical Generation

During inference, the dual-timestep formulation enables sequential chaining of the learned capabilities:

Stage 1: Depth Generation (Physical Reasoning). Initialize $\mathbf{z}^d, \mathbf{z}^v \sim \mathcal{N}(\mathbf{0}, \mathbf{I})$. Execute the DDIM sampling loop targeting only the depth stream (τ_v fixed at T_{max}). The model operates in Mode I, synthesizing a clean depth latent $\hat{\mathbf{z}}^d$ from the control inputs \mathbf{P} and camera motion \mathbf{W} . Throughout this stage, the RGB noise \mathbf{z}^v is held constant.

Stage 2: Appearance Synthesis (Neural Rendering). Fix the depth latent to $\hat{\mathbf{z}}^d$ (setting $\tau_d = 0$) and re-initialize \mathbf{z}^v with fresh noise. Run a second DDIM loop targeting the video stream, with the model operating in Mode II. The generated depth serves as a fixed geometric blueprint for rendering.

This hierarchical pipeline offers **interpretability**: the intermediate depth $\hat{\mathbf{D}}$ provides a verifiable 3D scene layout that users can inspect before committing to the expensive rendering stage. It also provides a natural editing interface—users may modify the predicted depth (e.g., removing or repositioning agents) and re-render with consistent appearance.

4 Experiments

Training Details. We fine-tune CogVideoX1.5-5B-I2V [49] on 8 NVIDIA H100 GPUs with DeepSpeed ZeRO Stage-2 [33] in `bf16` mixed precision. We use AdamW [26] with learning rate 1×10^{-5} , $(\beta_1, \beta_2) = (0.9, 0.95)$, weight decay 1×10^{-4} , and 100 warmup steps. Each sample consists of 33 frames at 320×480 resolution (stride 2). We train for 10 epochs with an effective batch size of 8.

Datasets. We primarily evaluate on **autonomous driving** using sequences from Waymo [36], Driving Dojo [44], and YouTube. To validate generality, we additionally evaluate on **Physion** [2] (rigid-body physics) and **Jaco Play** [11] (robotic manipulation).

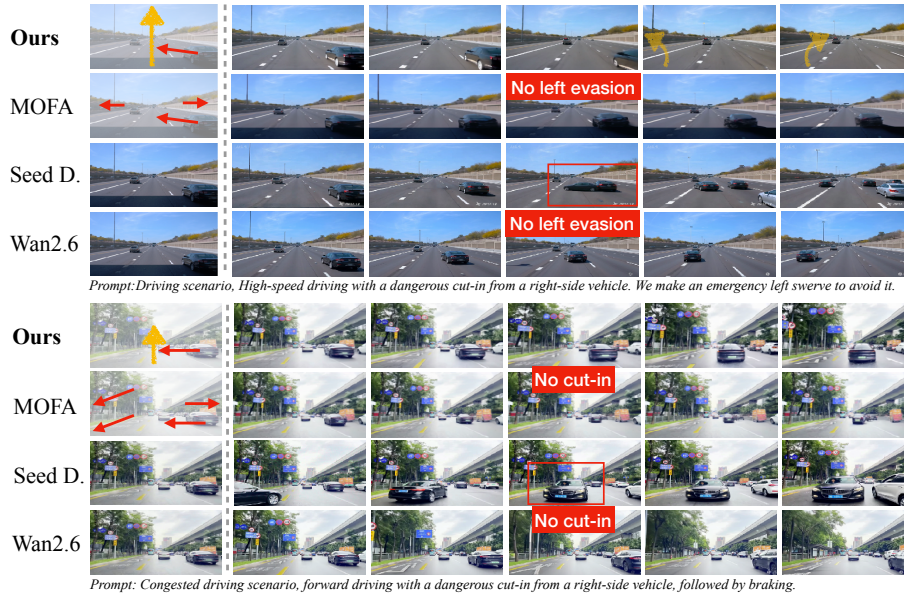


Fig. 3: Comparison with state-of-the-art models in synthesizing cut-in and evasive driving scenarios. While the leading closed-source models (Seed Dance2.0, Wan2.6) rely on text prompts, trajectory-controllable baselines like MOFA-Video require object trajectories coupled with scene trajectories to simulate camera movement. Our method **Motion Forcing**, however, effectively captures these complex dynamics given only the initial ego and object motion trajectories.

Table 1: Quantitative results on the Waymo dataset. One-stage* refers to the single-stage version of Motion Forcing, which directly generates RGB frames without intermediate depth.

Methods	MOFA-Video	Seed Dance2.0	Wan2.6	One-stage*	Ours
FVD ↓	272.6	112.5	118.3	152.4	157.8
FVMD ↓	421.3	345.6	316.2	218.4	205.2
Physics-IQ ↑	21.6	30.5	31.2	28.7	33.2

Evaluation Metrics. We report results on 100 Waymo [36] test videos using: (1) FVD [39] for distributional similarity, (2) FVMD [24] for temporal motion coherence, and (3) Physics-IQ [29] for physical plausibility.

4.1 Comparisons with the State-of-the-art Methods

Real-world Driving Video Generation. As shown in Tab. 1, we compare against MOFA-Video [31], closed-source models (Seed Dance2.0 [37], Wan2.6 [38]), and a one-stage variant on the Waymo test set. Seed Dance2.0 and Wan2.6 achieve substantially lower FVD (112.5 and 118.3) due to large-scale pretraining, yet

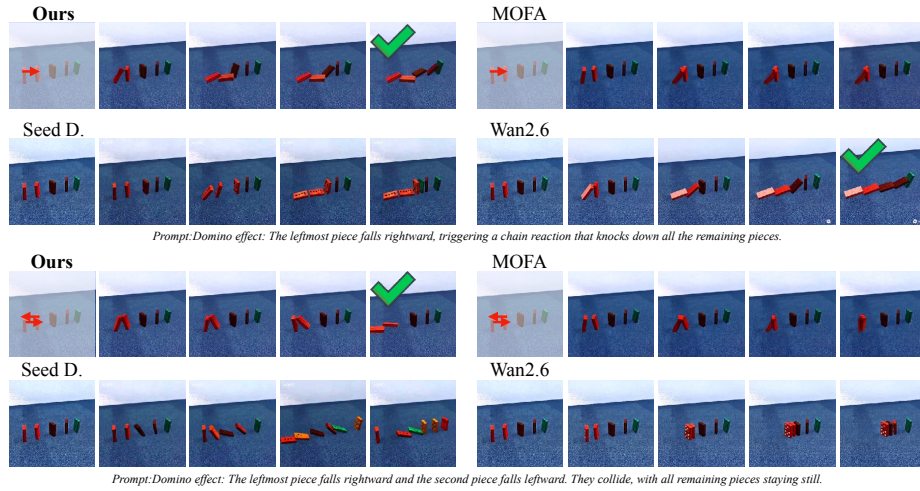


Fig. 4: Validation of physical capabilities. ✓ indicate physically coherent. MOFA-Video is fine-tuned on our exact dataset for fairness. As the control commands become more complex, only our method maintains stable and physically coherent generation.

our method significantly outperforms all baselines on motion coherence (FVMD 205.2) and physical plausibility (Physics-IQ 33.2). The one-stage variant achieves slightly lower FVD (152.4) but inferior FVMD (218.4) and Physics-IQ (28.7)—even below Seed Dance2.0 and Wan2.6—confirming that intermediate depth is critical for motion coherence. MOFA-Video performs worst across all metrics. Qualitatively (Fig. 3), text-conditioned models struggle with precise spatial dynamics, and MOFA-Video degrades under complex multi-agent interactions due to the mismatch between sparse optical flow and softmax splatting. Our method faithfully captures ego-object interplay from sparse initial trajectories, producing realistic lane-change and evasive maneuvers.

Generalization to Physics Scenarios. To validate the generality of our framework beyond driving, we evaluate on the Physion [2] dataset. As shown in Fig. 4, when physical interactions grow more complex (*e.g.*, multi-object collisions in domino scenarios), MOFA-Video—even fine-tuned on our dataset—fails to maintain physical coherence, whereas Motion Forcing consistently produces plausible collision dynamics, confirming that our hierarchy effectively transfers to general physics scenarios.

Generalization to Robotic Manipulation. We further validate on the Jaco Play [11] dataset by providing directional inputs to control robotic hand motions for grasping and object manipulation. As shown in Fig. 6, our model flexibly guides the robotic arm and grasped objects in specified directions, confirming the flexibility of our point-based control primitive across domains.

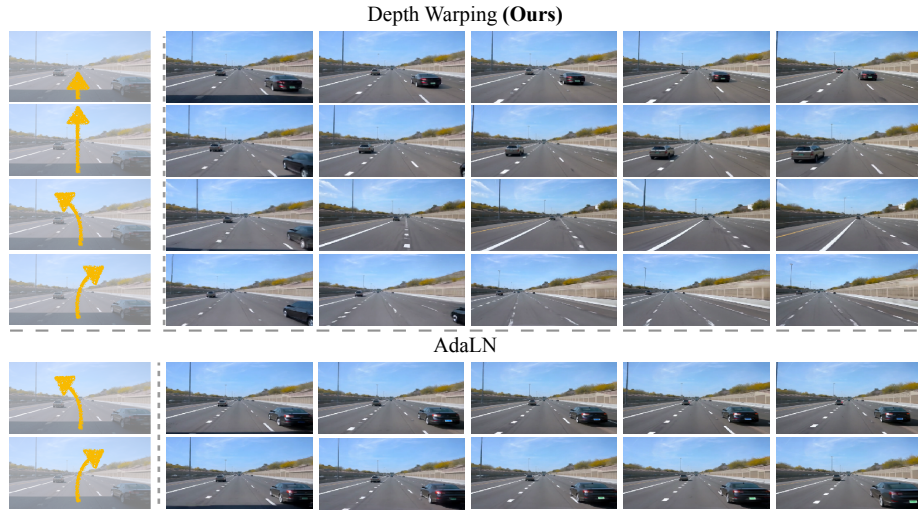


Fig. 5: Qualitative comparison of ego motion control. Compared to the baseline AdaLN approach, our **Depth Warping-based** method demonstrates significantly superior accuracy and flexibility in controlling both the direction and speed.

4.2 Ablation Study

We conduct comprehensive ablations on the Waymo test set to validate our key design choices, as summarized in Tab. 2.

Intermediate Motion Representation. Depth substantially outperforms segmentation (FVD 167.0, Physics-IQ 29.7) and optical flow (FVD 173.0, Physics-IQ 28.4). Depth encodes continuous 3D geometry—surface distances, occlusion ordering, and spatial relationships—that is indispensable for motion reasoning, while optical flow lacks 3D awareness and segmentation discards continuous spatial structure.

Object Motion Embedding. Replacing our instance flow with softmax splatting [31] has modest impact on FVD (160.3) but substantially degrades FVMD

Table 2: Ablation studies on the Waymo test set. Each row replaces one component of Motion Forcing with the specified alternative.

Methods	FVD↓	FVMD↓	Physics-IQ↑
Motion Forcing	157.8	205.2	33.2
Motion Representation			
Segmentation	167.0	228.8	29.7
Optical Flow	173.0	224.3	28.4
Object Motion Embedding			
Softmax Splatting [31]	160.3	251.7	28.5
Ego Motion Encoding			
AdaLN	159.6	243.8	29.1

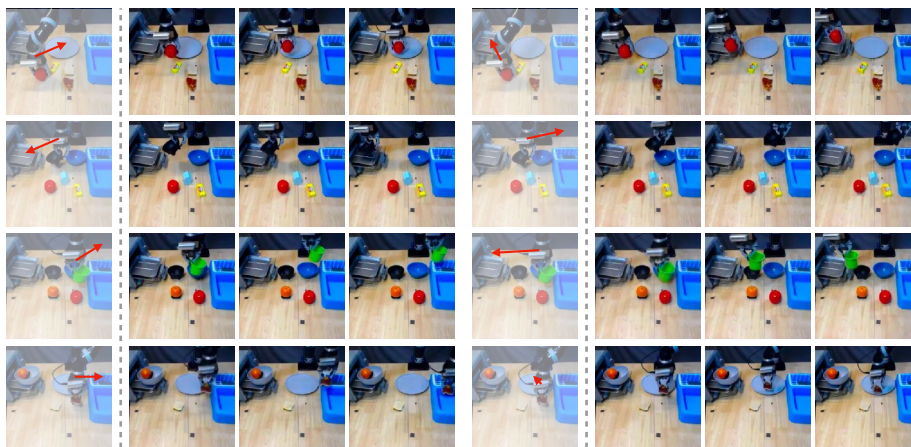


Fig. 6: Controllable robotic hand manipulation. By providing different motion control inputs, our model can flexibly control the movement of the robotic arm and the grasped object in specified directions.

(from 205.2 to 251.7) and Physics-IQ (from 33.2 to 28.5), as coarse pixel-level warping struggles to preserve temporal coherence in multi-body dynamics.

Ego Motion Encoding. As shown in Tab. 2 and Fig. 5, replacing depth warping with AdaLN has limited effect on FVD (159.6) but markedly degrades FVMD (from 205.2 to 243.8) and Physics-IQ (from 33.2 to 29.1), confirming that spatially explicit, pixel-aligned 6-DoF conditioning is essential for motion coherence and physical reasoning.

5 Conclusion and Limitation

We presented Motion Forcing, a decoupled framework that stabilizes the trilemma of visual quality, physical consistency, and controllability in complex scenes. By decomposing generation into physical reasoning and neural rendering via a “Point-Shape-Appearance” hierarchy with depth as the intermediate representation, our method bridges the gap between sparse control and dense video while enabling precise camera and object control through depth warping and instance flow. With Masked Point Recovery for active physical reasoning, Motion Forcing achieves state-of-the-art motion coherence and physical plausibility on autonomous driving benchmarks with strong generalization to physics simulation and robotics.

Limitation. Despite strong performance in common driving scenarios, our model still degrades in scenes with dense non-motorized traffic (*e.g.*, crowds of pedestrians and cyclists), where sparse point control struggles to capture diverse motion patterns of numerous small agents. Highly occluded multi-agent interactions also remain challenging, as the depth representation may fail to resolve occlusion ordering when multiple vehicles overlap significantly.

References

1. Bansal, H., Lin, Z., Xie, T., Zong, Z., Yarom, M., Bitton, Y., Jiang, C., Sun, Y., Chang, K.W., Grover, A.: Videophy: Evaluating physical commonsense for video generation (2024), <https://arxiv.org/abs/2406.03520>
2. Bear, D.M., Wang, E., Mrowca, D., Binder, F.J., Tung, H.Y.F., Pramod, R., Holdaway, C., Tao, S., Smith, K., Sun, F.Y., et al.: Physion: Evaluating physical prediction from vision in humans and machines. arXiv preprint arXiv:2106.08261 (2021)
3. Blattmann, A., Dockhorn, T., Kulal, S., Mendelevitch, D., Kilian, M., Lorenz, D., Levi, Y., English, Z., Voleti, V., Letts, A., et al.: Stable video diffusion: Scaling latent video diffusion models to large datasets. arXiv preprint arXiv:2311.15127 (2023)
4. Cai, S., Ceylan, D., Gadelha, M., Huang, C.H., Wang, T., Wetzstein, G.: Generative rendering: Controllable 4d-guided video generation with 2d diffusion models. In: CVPR (2024)
5. cerspense: zeroscope_v2. https://huggingface.co/cerspense/zeroscope_v2_576w (2023), accessed: 2023-02-03
6. Chen, A., Zheng, W., Wang, Y., Zhang, X., Zhan, K., Jia, P., Keutzer, K., Zhang, S.: Geodrive: 3d geometry-informed driving world model with precise action control. arXiv preprint arXiv:2505.22421 (2025)
7. Chen, B., Martí Monsó, D., Du, Y., Simchowitz, M., Tedrake, R., Sitzmann, V.: Diffusion forcing: Next-token prediction meets full-sequence diffusion. *Advances in Neural Information Processing Systems* **37**, 24081–24125 (2024)
8. Chen, H., Xia, M., He, Y., Zhang, Y., Cun, X., Yang, S., Xing, J., Liu, Y., Chen, Q., Wang, X., et al.: Videocrafter1: Open diffusion models for high-quality video generation. arXiv preprint arXiv:2310.19512 (2023)
9. Chen, H., Zhang, Y., Cun, X., Xia, M., Wang, X., Weng, C., Shan, Y.: Videocrafter2: Overcoming data limitations for high-quality video diffusion models (2024)
10. Chen, Z., Xu, T., Wu, L., Wang, L., Yan, D., You, Z., Luo, W., Zhang, G., Chen, Y.: Stance: Motion coherent video generation via sparse-to-dense anchored encoding. arXiv preprint arXiv:2510.14588 (2025)
11. Dass, S., Yapeter, J., Zhang, J., Zhang, J., Pertsch, K., Nikolaidis, S., Lim, J.J.: Clvr jaco play dataset (2023), https://github.com/clvr-ai/clvr_jaco_play_dataset
12. Escontrela, A., Adeniji, A., Yan, W., Jain, A., Peng, X.B., Goldberg, K., Lee, Y., Hafner, D., Abbeel, P.: Video prediction models as rewards for reinforcement learning. arXiv preprint arXiv:2305.14343 (2023)
13. Guo, Y., Yang, C., Rao, A., Wang, Y., Qiao, Y., Lin, D., Dai, B.: Animatediff: Animate your personalized text-to-image diffusion models without specific tuning. arXiv preprint arXiv:2307.04725 (2023)
14. Hong, W., Ding, M., Zheng, W., Liu, X., Tang, J.: Cogvideo: Large-scale pretraining for text-to-video generation via transformers. arXiv preprint arXiv:2205.15868 (2022)
15. Hu, A., Russell, L., Yeo, H., Murez, Z., Fedoseev, G., Kendall, A., Shotton, J., Corrado, G.: Gaia-1: A generative world model for autonomous driving. arXiv preprint arXiv:2309.17080 (2023)
16. Hu, L., Gao, X., Zhang, P., Sun, K., Zhang, B., Bo, L.: Animate anyone: Consistent and controllable image-to-video synthesis for character animation. arXiv preprint arXiv:2311.17117 (2023)

17. Kang, B., Yue, Y., Lu, R., Lin, Z., Zhao, Y., Wang, K., Huang, G., Feng, J.: How far is video generation from world model: A physical law perspective (2024), <https://arxiv.org/abs/2411.02385>
18. Ko, P.C., Mao, J., Du, Y., Sun, S.H., Tenenbaum, J.B.: Learning to Act from Actionless Videos through Dense Correspondences. arXiv:2310.08576 (2023)
19. Kong, W., Tian, Q., Zhang, Z., Min, R., Dai, Z., Zhou, J., Xiong, J., Li, X., Wu, B., Zhang, J., et al.: Hunyuanvideo: A systematic framework for large video generative models. arXiv preprint arXiv:2412.03603 (2024)
20. Kundur Satish, S.N., Jaiswal, D., Chen, H., Bakshi, A.: Physvideogenerator: Towards physically aware video generation via latent physics guidance. arXiv preprint arXiv:2601.03665 (2026)
21. Li, X., Zhang, Y., Ye, X.: Drivingdiffusion: Layout-guided multi-view driving scene video generation with latent diffusion model. arXiv preprint arXiv:2310.07771 (2023)
22. Lipman, Y., Chen, R.T., Ben-Hamu, H., Nickel, M., Le, M.: Flow matching for generative modeling. arXiv preprint arXiv:2210.02747 (2022)
23. Liu, F., Wang, H., Yao, S., Zhang, S., Zhou, J., Duan, Y.: Physics3d: Learning physical properties of 3d gaussians via video diffusion. arXiv preprint arXiv:2406.04338 (2024)
24. Liu, J., Qu, Y., Yan, Q., Zeng, X., Wang, L., Liao, R.: Fréchet video motion distance: A metric for evaluating motion consistency in videos. arXiv preprint arXiv:2407.16124 (2024)
25. Liu, S., Ren, Z., Gupta, S., Wang, S.: Physgen: Rigid-body physics-grounded image-to-video generation. In: European Conference on Computer Vision. pp. 360–378. Springer (2024)
26. Loshchilov, I., Hutter, F.: Decoupled weight decay regularization. In: International Conference on Learning Representations (2019), <https://openreview.net/forum?id=Bkg6RiCqY7>
27. Lu, H., Ma, Z., Jiang, G., Ge, W., Li, B., Cai, Y., Zheng, W., Zhang, Y., Chen, Y.: 4d driving scene generation with stereo forcing. arXiv preprint arXiv:2509.20251 (2025)
28. Meng, F., Liao, J., Tan, X., Shao, W., Lu, Q., Zhang, K., Cheng, Y., Li, D., Qiao, Y., Luo, P.: Towards world simulator: Crafting physical commonsense-based benchmark for video generation. arXiv preprint arXiv:2410.05363 (2024)
29. Motamed, S., Culp, L., Swersky, K., Jaini, P., Geirhos, R.: Do generative video models understand physical principles? arXiv preprint arXiv:2501.09038 (2025)
30. Namekata, K., Bahmani, S., Wu, Z., Kant, Y., Gilitschenski, I., Lindell, D.B.: Sg-i2v: Self-guided trajectory control in image-to-video generation. arXiv preprint arXiv:2411.04989 (2024)
31. Niu, M., Cun, X., Wang, X., Zhang, Y., Shan, Y., Zheng, Y.: Mofa-video: Controllable image animation via generative motion field adaptations in frozen image-to-video diffusion model. arXiv preprint arXiv:2405.20222 (2024)
32. OpenAI: Video generation models as world simulators. OpenAI Blog (2024), <https://openai.com/research/video-generation-models-as-world-simulators>
33. Rajbhandari, S., Rasley, J., Ruwase, O., He, Y.: Zero: Memory optimizations toward training trillion parameter models. In: SC20: International Conference for High Performance Computing, Networking, Storage and Analysis. pp. 1–16. IEEE (2020)
34. Ren, X., Shen, T., Huang, J., Ling, H., Lu, Y., Nimier-David, M., Müller, T., Keller, A., Fidler, S., Gao, J.: Gen3c: 3d-informed world-consistent video generation with precise camera control. In: Proceedings of the Computer Vision and Pattern Recognition Conference. pp. 6121–6132 (2025)

35. Rombach, R., Blattmann, A., Lorenz, D., Esser, P., Ommer, B.: High-resolution image synthesis with latent diffusion models. In: Proceedings of the IEEE/CVF conference on computer vision and pattern recognition. pp. 10684–10695 (2022)
36. Sun, P., Kretschmar, H., Dotiwalla, X., Chouard, A., Patnaik, V., Tsui, P., Kennedy, J., Todd, C., et al.: Scalability in perception for autonomous driving: Waymo open dataset. In: Proceedings of the IEEE/CVF conference on computer vision and pattern recognition. pp. 2446–2454 (2020)
37. Team, B.S.: Seedance 1.0: Exploring the boundaries of video generation models. arXiv preprint arXiv:2506.09113 (2025)
38. Team, W.: Wan: Open and advanced large-scale video generative models. arXiv preprint arXiv:2503.20314 (2025), <https://arxiv.org/abs/2503.20314>
39. Unterthiner, T., van Steenkiste, S., Kurach, K., Marinier, R., Michalski, M., Gelly, S.: Towards accurate generative models of video: A new metric and challenges (2019), <https://arxiv.org/abs/1812.01717>
40. Wang, J., Chen, M., Karaev, N., Vedaldi, A., Rupprecht, C., Novotny, D.: Vggt: Visual geometry grounded transformer. In: Proceedings of the Computer Vision and Pattern Recognition Conference. pp. 5294–5306 (2025)
41. Wang, J., Yuan, H., Chen, D., Zhang, Y., Wang, X., Zhang, S.: Modelscope text-to-video technical report. arXiv preprint arXiv:2308.06571 (2023)
42. Wang, X., Zhu, Z., Huang, G., Chen, X., Zhu, J., Lu, J.: Drivedreamer: Towards real-world-driven world models for autonomous driving. arXiv preprint arXiv:2309.09777 (2023)
43. Wang, X., Zhu, Z., Huang, G., Wang, B., Chen, X., Lu, J.: Worlddreamer: Towards general world models for video generation via predicting masked tokens. arXiv preprint arXiv:2401.09985 (2024)
44. Wang, Y., Cheng, K., He, J., Wang, Q., Dai, H., Chen, Y., Xia, F., Zhang, Z.: Drivingdojo dataset: Advancing interactive and knowledge-enriched driving world model. In: Advances in Neural Information Processing Systems (2024)
45. Wu, H., Jing, Y., Cheang, C., Chen, G., Xu, J., Li, X., Liu, M., Li, H., Kong, T.: Unleashing large-scale video generative pre-training for visual robot manipulation. In: International Conference on Learning Representations (2024)
46. Wu, W., Li, Z., Gu, Y., Zhao, R., He, Y., Zhang, D.J., Shou, M.Z., Li, Y., Gao, T., Zhang, D.: Draganything: Motion control for anything using entity representation (2024), <https://arxiv.org/abs/2403.07420>
47. Yang, J., Gao, S., Qiu, Y., Chen, L., Li, T., Dai, B., Chitta, K., Wu, P., Zeng, J., Luo, P., et al.: Generalized predictive model for autonomous driving. In: Proceedings of the IEEE/CVF Conference on Computer Vision and Pattern Recognition. pp. 14662–14672 (2024)
48. Yang, Y., Fan, L., Shi, Z., Peng, J., Wang, F., Zhang, Z.: Neoverse: Enhancing 4d world model with in-the-wild monocular videos. arXiv preprint arXiv:2601.00393 (2026)
49. Yang, Z., Teng, J., Zheng, W., Ding, M., Huang, S., Xu, J., Yang, Y., Hong, W., Zhang, X., Feng, G., et al.: Cogvideox: Text-to-video diffusion models with an expert transformer. arXiv preprint arXiv:2408.06072 (2024)
50. Yin, S., Wu, C., Liang, J., Shi, J., Li, H., Ming, G., Duan, N.: Dragnuwa: Fine-grained control in video generation by integrating text, image, and trajectory. arXiv preprint arXiv:2308.08089 (2023)
51. Zeng, Y., Wei, G., Zheng, J., Zou, J., Wei, Y., Zhang, Y., Li, H.: Make pixels dance: High-dynamic video generation. arXiv:2311.10982 (2023)

52. Zhang, D.J., Li, D., Le, H., Shou, M.Z., Xiong, C., Sahoo, D.: Moonshot: Towards controllable video generation and editing with multimodal conditions. arXiv preprint arXiv:2401.01827 (2024)
53. Zhang, D.J., Wu, J.Z., Liu, J.W., Zhao, R., Ran, L., Gu, Y., Gao, D., Shou, M.Z.: Show-1: Marrying pixel and latent diffusion models for text-to-video generation. arXiv preprint arXiv:2309.15818 (2023)
54. Zhang, K., Xiao, C., Mei, Y., Xu, J., Patel, V.M.: Think before you diffuse: Llms-guided physics-aware video generation. arXiv preprint arXiv:2505.21653 (2025)
55. Zhang, T., Yu, H.X., Wu, R., Feng, B.Y., Zheng, C., Snavely, N., Wu, J., Freeman, W.T.: PhysDreamer: Physics-based interaction with 3d objects via video generation. arxiv (2024)
56. Zhang, X., Liao, J., Zhang, S., Meng, F., Wan, X., Yan, J., Cheng, Y.: Videorepa: Learning physics for video generation through relational alignment with foundation models. arXiv preprint arXiv:2505.23656 (2025)
57. Zhao, G., Wang, X., Zhu, Z., Chen, X., Huang, G., Bao, X., Wang, X.: Drivedreamer-2: Llm-enhanced world models for diverse driving video generation. arXiv preprint arXiv:2403.06845 (2024)
58. Zhuang, S., Li, K., Chen, X., Wang, Y., Liu, Z., Qiao, Y., Wang, Y.: Vlogger: Make your dream a vlog. arXiv preprint arXiv:2401.09414 (2024)